

The role of soluble Fe(III) in the cycling of iron and sulfur in coastal marine sediments

Elizabeth Carey and Martial Taillefert¹

School of Earth and Atmospheric Sciences, Georgia Institute of Technology, Atlanta, Georgia 30332-0340

Abstract

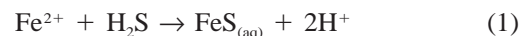
In marine sediments, Fe(III) is found predominantly as a solid. Recently, however, soluble species of Fe³⁺ complexed by natural organic ligands have been detected in coastal marine sediments with voltammetric microelectrodes. The role of soluble Fe³⁺ complexes in diagenesis is unknown. In anoxic conditions, soluble Fe³⁺ can effectively oxidize FeS₂ and recycle iron and sulfur for use as terminal electron acceptors during natural organic matter (NOM) degradation. Alternatively, soluble Fe³⁺ complexes can catalyze the formation of FeS and FeS₂ through the rapid chemical reduction of Fe³⁺ by dissolved sulfide. To better understand the role of soluble Fe³⁺ in the transformation of iron and sulfur in marine sediments, we incubated the first few centimeters of unvegetated salt marsh sediment in plug-flow reactors. Microbial iron reduction seemed to prevail in suboxic conditions, but sulfate reduction outcompeted microbial iron reduction in the presence of reactive organic metabolites. The dominance of sulfate reduction led to the complete removal of reactive iron oxides by precipitation of FeS. Experiments mimicking the enrichment of soluble Fe³⁺ complexes in reduced sediments show that soluble Fe³⁺ does not reoxidize FeS and pyrite; rather, it promotes pyrite precipitation by enhancing sulfate reduction via complex bacterial interactions. The rate of pyrite formation in the presence of soluble Fe³⁺ is much higher than previously reported in the literature, suggesting that soluble Fe³⁺ might promote alternative pathways for microbial degradation of NOM that ultimately results in the immobilization of Fe and S as reduced iron sulfide minerals.

The biogeochemical processes involved in the transformation of natural organic matter (NOM) in salt marsh sediments are poorly understood mainly because the flux of organic carbon and physical processes (i.e., tidal forcing and bioturbation) in these environments lead to high biogeochemical complexity. It is generally recognized that sulfate reduction accounts for up to 90% of the NOM oxidation in salt marsh sediments (Jorgensen 1982; Howarth 1984; King et al. 1985). Recently, however, the significance of microbial iron reduction on the remineralization of NOM in salt marsh sediments has been demonstrated (Jacobsen 1994; Kostka and Luther 1995; Lowe et al. 2000; Koretsky et al. 2003), and the mechanisms of microbial iron reduction are currently being investigated (e.g., Myers and Myers 1993; Lovley and Woodward 1996; DiChristina et al. 2002).

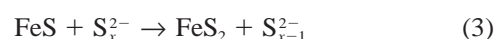
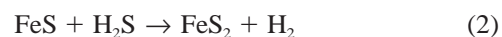
The reactivity of ferric iron in marine sediments has been assessed on the premise that it exists in a precipitated or colloidal form. However, more readily bioavailable soluble Fe³⁺ should accelerate the mineralization of organic carbon, as well as other reactions involving iron. Evidence for the existence of soluble Fe³⁺ in salt marsh sediments has been documented (Luther et al. 1992; Luther et al. 1996). More recently, soluble organic complexes of Fe³⁺ were detected by voltammetry with gold-mercury amalgam (Au/Hg) mi-

croelectrodes (Taillefert et al. 2000). Such complexes (hereafter referred to as soluble organic Fe^(III)) have since been found ubiquitously in anoxic coastal marine sediments (Taillefert et al. 2000, 2002*a,b*; Bull and Taillefert 2001; Neuhuber 2003). The mechanisms by which soluble Fe³⁺ forms are still under investigation. Possible explanations include chemical oxygenation (Neuhuber 2003) and microbial oxidation of Fe²⁺ in the presence of organic ligands or nonreductive dissolution of solid iron oxides, preferably by organic bidentate ligands containing at least one oxygen atom (Luther et al. 1992). In the latter mechanism, the organic ligands could be produced by iron-reducing bacteria to dissolve iron oxides prior to reduction (Lovley and Woodward 1996; Nevin and Lovley 2002).

Rates of microbial iron reduction with soluble Fe³⁺ are much higher than with solid Fe³⁺ (Arnold et al. 1988; Lovley and Woodward 1996; Dollhopf et al. 2000) and inversely proportional to the strength of the organic complex (Haas and DiChristina 2002). Similarly, soluble organic Fe^(III) is rapidly reduced by dissolved sulfide (Taillefert et al. 2000). The reduction of these complexes by dissolved sulfide is followed by the formation of soluble FeS (Eq. 1; Theberge and Luther 1997; Taillefert et al. 2000),



which is often found with the onset of dissolved sulfide in coastal sediments (Taillefert et al. 2000, 2002*a,b*; Bull and Taillefert 2001). It is proposed that FeS_(aq) is an intermediate in the formation of amorphous FeS (Rickard 1995), and eventually pyrite, through reaction with H₂S at low pH (Eq. 2; Rickard and Luther 1997) or polysulfides at high pH (Eq. 3; Luther 1991).



In turn, soluble Fe³⁺ has been found to effectively oxidize

¹ Corresponding author (mtaillef@eas.gatech.edu).

Acknowledgments

We thank Richard A. Jahnke and the staff of the Skidaway Institute of Oceanography, who facilitated our work in the Skidaway salt marsh by allowing us to use their facilities. Gwendolyn Bristow, Stephanie Chow, Stephanie Neuhuber, and Dian Putrasahan provided some of the analyses conducted in this study. The comments of two anonymous reviewers improved the manuscript. This project was partially funded by a type-G Petroleum Research Fund grant from the American Chemical Society (PRF 38898-G2) and the CA-REER program from the National Science Foundation (OCE-0239376).

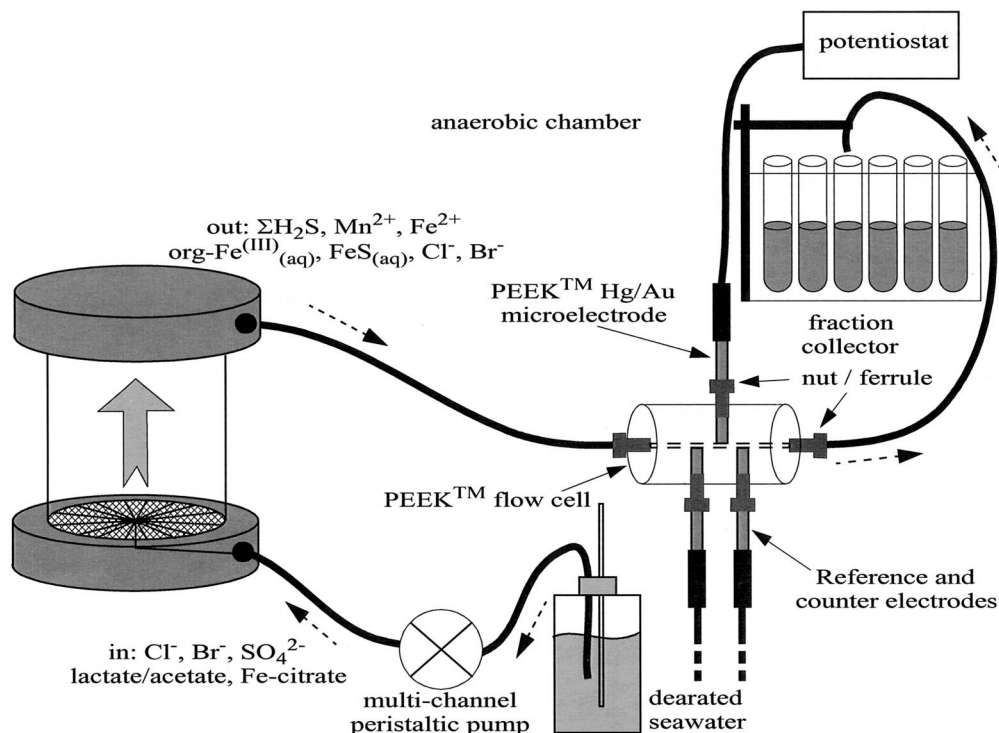
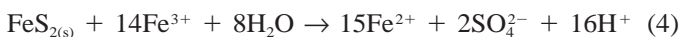


Fig. 1. Illustration of a plug-flow reactor (PFR) and the experimental set-up. Three reactors were used for these incubations. After day 63, the reactors were kept in an anaerobic chamber that was continuously purged with N_2 . The degassed seawater enters the PFR from the base and is directed through a mesh screen and a $0.45\text{-}\mu\text{m}$ membrane. It passes through a flow cell that contains a voltammetric electrode to monitor the composition of the pore waters and is sampled periodically with a fraction collector.

pyrite (Eq. 4) in acidic conditions (Singer and Stumm 1970) or at circumneutral pH if Fe^{3+} is complexed by an organic ligand (Luther et al. 1992).



Therefore, soluble organic $Fe^{(III)}$ might enhance pyrite formation if dissolved sulfide or polysulfides are in excess or oxidize pyrite in the absence of dissolved sulfide. In the former case, the rate of precipitation of pyrite could be limited by sulfate reduction, and soluble organic $Fe^{(III)}$ might prevent efficient recycling of two important terminal electron acceptors in microbial NOM oxidation. In the latter case, soluble organic $Fe^{(III)}$ might oxidize pyrite efficiently if sulfate reduction is not active and recycle iron and sulfur for more microbial iron and sulfate reduction.

In this study, small sediment plug-flow reactors were employed to constrain the reaction mechanisms by which iron and sulfur cycle in anoxic salt marsh sediments. Particular attention was given to the effect of soluble organic $Fe^{(III)}$ on the formation and dissolution of sulfur minerals.

Experimental design

Three plug-flow reactors were filled with sediment collected from the Salt Marsh Environmental Research Facility (SERF) at the Skidaway Institute of Oceanography (SkIO) on Skidaway Island, Georgia, in the spring of 2002. The

reactors consist of a cylinder ~ 8 cm long with an inside diameter of 3.8 cm (Fig. 1). On both sides of the cylinder are identical covers that screw onto the top and base. Within each cover sits an O-ring, a plastic mesh screen, and a $0.45\text{-}\mu\text{m}$ filter (Micro Filtration Systems). The base of the reactor is designed such that the water is funneled through an opening surrounded by radial grooves to direct the solution in a way that encompasses the entire surface area of the base of the reactor. It is then forced upward through the mesh screen and $0.45\text{-}\mu\text{m}$ filter and into the sediment, where it flows through the reactors. The pore waters are then filtered in situ before exiting the top of the reactors. The effluent was pumped through a homemade PEEK™ flow cell ~ 7.4 cm in length that can accommodate a PEEK Au/Hg microelectrode (Luther et al. 2002). The counter and reference electrodes were stationed in a catchment at the outlet of the flow cell during measurements to provide the necessary electrical contact between the three electrodes. After the flow cell, the pore waters were sampled with a fraction collector (Eldex) in polypropylene Falcon® tubes at a rate of two samples per day. Each day, one of the samples was acidified to pH 2 with concentrated trace metal-grade HCl (Fisher Scientifics) and stored at 4°C ; the other sample was immediately analyzed for pH and frozen until further analysis.

Artificial seawater (ASW; Dickson 1993) was prepared with reagent-grade salts in Milli-Q water and was continuously degassed with UHP compressed argon while fed

through the plug-flow reactors via a high-precision multi-channel pump (IsmaTec®) at a rate of 1 ml h⁻¹. Previous tests conducted with sediment from the same site showed that channelization was not visually perceptible at such a low flow rate. Bromide was added to a concentration of 10 mmol L⁻¹ as a tracer of the transport processes through the reactors.

Redox conditions within the reactors changed over the course of this 396-day experiment in response to experimental manipulations. Three dominant regimes have been identified: Microaerobic conditions prevailed between 0 and 63 d when the reactors were exposed to ambient air while deaerated ASW was pumped through them. Under these conditions, some oxygen could have penetrated the reactors. Suboxic conditions prevailed between 63 and 120 d when the reactors were placed in an anaerobic chamber and dissolved sulfide was below detection limit. Finally, anoxic conditions (i.e., production of dissolved sulfide) began on day 120 and included the time between 120 and 174 d, during which an electron donor mixture (15 mmol L⁻¹ lactate and 15 mmol L⁻¹ acetic acid, pH 8.3) was injected into the reactors; the period between 290 and 366 d, during which a soluble organic Fe^(III) solution (500 μmol L⁻¹ ferric citrate) was pumped through the reactors; and the time between 366 and 396 d, during which ferric citrate in the inlet solution was replaced by a 500 μmol L⁻¹ sodium citrate solution.

Experiments to investigate the reactivity of ferric citrate with dissolved sulfide were conducted in a voltammetric cell stand (Analytical Instrument Systems) with the same electrode setup as for the in-line voltammetric measurements (see "In-line measurements"). For these experiments, a known volume of seawater was degassed and spiked with a ferric citrate solution to achieve a 500 μmol L⁻¹ final concentration. The solution was analyzed for soluble organic Fe^(III), aqueous FeS, Fe²⁺, and ΣH₂S (=H₂S + HS⁻ + S²⁻ + S⁰ + S_x²⁻) as a function of time before and after addition of dissolved sulfide to a final concentration of 20 μmol L⁻¹. The ΣH₂S and soluble organic Fe^(III) peaks were deconvoluted by minimizing the difference between analytical data and theoretical gaussian peaks of both species with mathematical software (PeakFit, Jandel Scientific).

Analytical methods

Effluent pore waters—Acidified pore-water samples were analyzed for both Fe²⁺ and total Fe by the ferrozine method modified after Stookey (1970). Total Fe was measured by reducing all dissolved Fe with hydroxylamine at pH 1 for 24 h before analysis of Fe²⁺. Acidified samples were also analyzed for total dissolved manganese (Mn_d) with graphite furnace atomic absorption spectroscopy and Zeeman background correction (Varian Spectra AA-600). The pH was determined in unacidified samples with an Orion pH electrode by measuring potential and temperature with a pH meter (Orion model 290Aplus). A Tris buffer (pH ~8) in 0.54 mol L⁻¹ NaCl (Dickson 1993) was used as a standard for all pH measurements, and pH was calculated from the Nernst equation. Salinity measurements were collected with a portable salinity refractometer (Fisher Scientific). Sulfate, bro-

midate, and chloride were analyzed by ion chromatography (Dionex, DX-300 series) equipped with a Dionex IonPac® AS4A chromatography column, AG4A guard column, and AMMS III suppressor. Samples and standards were diluted at 1:100 proportions before analysis.

In-line measurements—Voltammetric analyses were carried out in line in the flow cell with a computer-operated DLK-100A potentiostat (Analytical Instrument Systems), thus providing real-time data. One of the benefits of voltammetry is the ability to analyze multiple species simultaneously including O₂, H₂O₂, Fe²⁺, Mn²⁺, S₂O₃²⁻, ΣH₂S (=H₂S + HS⁻ + S²⁻ + S⁰ + S_x²⁻), soluble organic Fe^(III), and aqueous FeS (Taillefert and Luther 2000). Note that S⁰ in this analysis represents the dissolved fraction of total elemental sulfur S₈ (Wang et al. 1998). In addition to being able to measure several redox species at once during a potential scan, voltammetry benefits from low detection limits, fast analysis time, high reproducibility (Brendel and Luther 1995), in situ capability (Luther et al. 1998), and high spatial and temporal resolution (Taillefert et al. 2000; Bull and Taillefert 2001; Taillefert and Rozan 2002).

All voltammetric measurements were performed with Au/Hg solid-state microelectrodes fabricated as in Brendel and Luther (1995), a platinum counter electrode, and an Ag/AgCl reference electrode. The working microelectrodes consist of a 100-μm-diameter Au wire housed in 3-mm PEEK tubing connected via a copper conducting wire to a potentiostat. The Au surface was polished with diamond pastes of 15, 6, 1, and 0.25 μm (Buehler), mercury plated at -0.1 V in a Hg(NO₃)₂ solution, and then polarized at -9 V for 90 s to form a good amalgam between the Au and Hg (Brendel and Luther 1995). Finally, electrodes were tested first for quality and calibrated for dissolved oxygen by linear sweep voltammetry, then Mn²⁺ by cathodic square wave voltammetry (CSWV) in degassed seawater. Both the O₂ (minimum detection limit (MDL) ≈ 4 μmol L⁻¹) and Mn²⁺ (MDL ≈ 15 μmol L⁻¹ in seawater) calibrations were run from -0.1 to -1.75 V with a scan rate of 200 mV s⁻¹. A preconditioning potential of -0.1 V for 10 s was applied to all O₂ and Mn²⁺ measurements to clean the surface of the microelectrodes between measurements (Brendel and Luther 1995). The Mn²⁺ calibration curves were used to elucidate the concentrations of other species with the pilot ion method (Brendel and Luther 1995).

Ferrous Fe (Brendel and Luther 1995; MDL ≈ 25 μmol L⁻¹ in seawater), soluble organic Fe^(III) (Taillefert et al. 2000), and aqueous FeS (Theberge and Luther 1997) were always measured by CSWV under the same conditions used for Mn²⁺, except that a cleaning step at -0.9 V for 10 s was added to measure soluble organic Fe^(III) and aqueous FeS. This step ensured that any soluble organic Fe^(III) and aqueous FeS adsorbed at the electrode surface was removed before the next measurement (Theberge and Luther 1997; Taillefert et al. 2000). Soluble ferric iron can only be measured by voltammetry at circumneutral pH if it is complexed by an organic ligand (Taillefert et al. 2000). Several unknown organic Fe^(III) complexes could be detected simultaneously at the microelectrode because NOM contains a multitude of uncharacterized organic ligands. The sensitivities of these

complexes have yet to be determined, and their concentrations are therefore reported in current intensities (Taillefert et al. 2000). Similarly, the stoichiometry of FeS is unknown (Theberge and Luther 1997), and current intensities are usually reported for these measurements. Cathodic square wave voltammetry was always used for low concentrations of sulfide with a cleaning potential of -0.9 V for 10 s followed by a preconditioning step at -0.1 V for 10 s (MDL ≈ 0.2 $\mu\text{mol L}^{-1}$). When sulfide concentrations were too high (i.e., >40 $\mu\text{mol L}^{-1}$), anodic square wave voltammetry was preferred (De Vitre et al. 1988).

Solid phase measurements—Small sediment samples were collected in triplicate in each reactor on days 0, 246, and 379 by opening the reactors in the anaerobic chamber. Except for the original sediment, the solid concentrations reported represent the average of the three reactors' triplicate measurements. Amorphous iron oxides and total reactive iron were determined in the solid sediment by the ascorbate and dithionite methods (Kostka and Luther 1994). The ascorbate reagent (0.2 mol L⁻¹ sodium citrate, 0.6 mol L⁻¹ sodium bicarbonate, and 0.1 mol L⁻¹ L-ascorbic acid, pH ~ 8) extracts only amorphous forms of Fe³⁺, whereas the dithionite extract (0.35 mol L⁻¹ ammonium acetate, 0.2 mol L⁻¹ sodium citrate, and 0.03 mol L⁻¹ sodium dithionite, pH ~ 4.8) dissolves amorphous iron oxides, acid volatile sulfide (AVS), and crystalline iron oxides, including magnetite, goethite, and to a lesser extent chlorite. Separate wet sediment samples were reacted with the ascorbate reagent at 25°C for ~ 24 h and with the dithionite reagent for ~ 4 h in a 60°C water bath. Samples were then filtered, diluted, and analyzed by the ferrozine method (Stookey 1970).

Pyrite (FeS₂) and AVS were extracted by the distillation methods described by Canfield et al. (1986) and Henneke et al. (1991), respectively. For AVS extractions, ~ 0.5 g of wet sediment was weighed into four distillation vessels. Concentrated HCl (3 mol L⁻¹) was added to each vessel through a nylon septum after the entire apparatus had been degassed with N₂ for at least 1 h. The volatile H₂S gas was distilled for 4 h at normal temperature with N₂ gas as carrier and trapped in a 1 mol L⁻¹ NaOH solution connected to the top of each distillation vessel. The nitrogen gas was continuously stripped of residual oxygen by a copper trap heated to 350°C thus preventing the rapid oxidation of HS⁻ (Miller 1986) trapped in the NaOH solution. An aliquot of this solution was then analyzed voltammetrically for $\Sigma\text{H}_2\text{S}$ in 0.5 mol L⁻¹ NaCl.

Before the FeS₂ extraction, the sediment was washed with acetone at room temperature for 24 h to remove elemental sulfur that could interfere with the pyrite measurements. The sediment was then dried, and ~ 0.5 g of sediment was added to four distillation vessels identical to those used in the AVS extraction. Pyrite was reduced to H₂S for ~ 2 h by a freshly prepared 1 mol L⁻¹ Cr²⁺ solution in a 2:1 volume ratio with 3 mol L⁻¹ trace metal-grade HCl. Reduced chromium reagent was prepared overnight by the Jones reaction: a CrCl₃·6H₂O (Sigma) solution was reduced by zinc granules amalgamated with 2% Hg(NO₃)₂·H₂O (Aldrich) in 2% trace metal-grade HCl. Similar to the AVS extraction, the reduced Cr²⁺/HCl mixture was added to each reaction vessel through

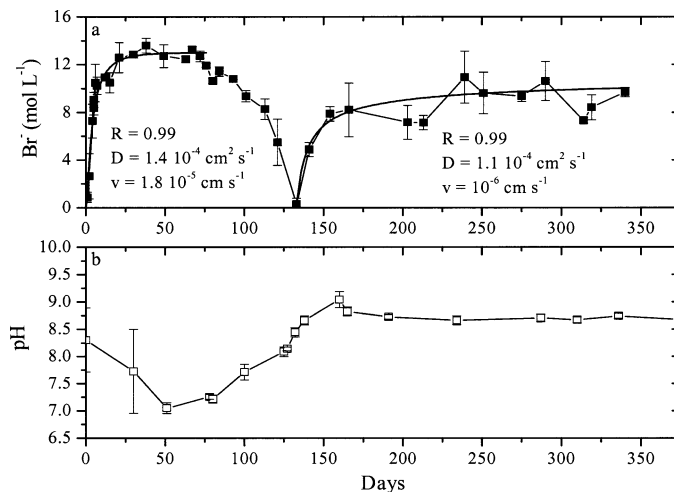


Fig. 2. (a) Average bromide concentration in the effluent of the three reactors as a function of time. Bromide was introduced in the input seawater at the beginning of the experiment and removed after 74 d. It was reintroduced on day 132 to determine whether the changes in the sediment composition affected the transport of dissolved constituents in the reactors. The plain line represents the bromide breakthrough curve modeled with the analytical solution to the one-dimensional advection–dispersion equation (Eq. 5). (b) Average pH as a function of time in the effluent of the three reactors. Error bars represent the standard deviations from the average measurements in the three reactors.

its nylon septum, and a 1 mol L⁻¹ NaOH solution served as the trap for dissolved sulfide produced during the reaction. An aliquot of the NaOH solution was then analyzed for sulfide by voltammetry.

Results

To study the role of soluble organic Fe^(III) on the cycling of iron and sulfur in salt marsh sediments, the sediment was manipulated in different ways. First, it was exposed to degassed seawater to determine what anaerobic process could be established. Then, organic compounds that are easily metabolized were injected into the reactors to activate sulfate reduction and precipitate iron and sulfur as FeS_(s) and pyrite. The reduced sediment was then exposed to ferric citrate in deaerated ASW to evaluate whether pyrite oxidation by soluble organic Fe^(III) was significant. Finally, a solution of sodium citrate was injected into the reactors to determine whether citrate or by-products of citrate metabolism could provide reducing power to sulfate-reducing bacteria. All the data reported in Figs. 2–6 represent the average and standard deviation for triplicate reactors.

Conservative tracer—Bromide was injected as a conservative tracer (Roychoudhury et al. 1998) to determine the dispersion coefficient and advection rate, as well as to establish the residence time of the influent seawater in the plug-flow reactors. It was removed from the input solution at 74 d and reintroduced at 132 d to determine whether the transport parameters remained constant with time. The average concentrations and standard deviations of bromide in

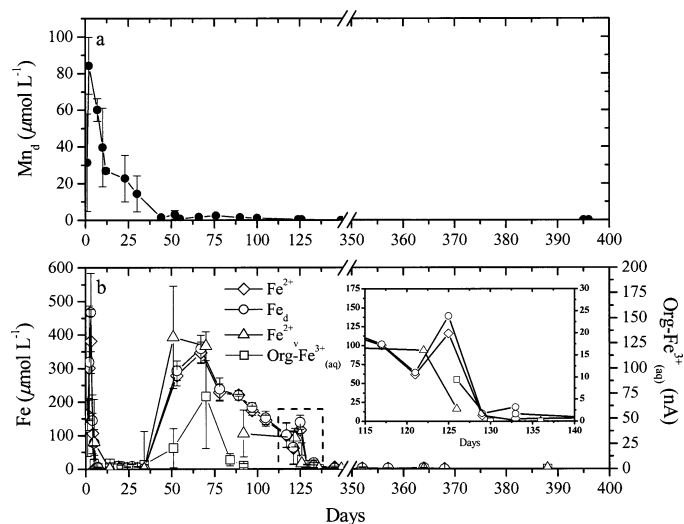


Fig. 3. (a) Average total dissolved Mn as a function of time in the effluent of the three reactors. Note the break in the x-axis from 150 to 350 d. (b) Average Fe speciation by colorimetry and voltammetry as a function of time in the three reactors. Open diamonds and triangles represent Fe^{2+} by the colorimetric and voltammetric methods, respectively; open circles represent total dissolved Fe (Fe_d); and open squares represent soluble organic $\text{Fe}^{(III)}$ determined by voltammetry. The standard deviations illustrate the variations between the three reactors. The inset displays the time period between days 115 and 125.

the three reactors as a function of time showed that bromide indeed behaved conservatively in the three reactors (Fig. 2a). However, the sediment seemed to change porosity over time, as indicated by the slightly smaller gradient in bromide concentration on reintroduction. Salinity and chloride remained essentially constant over time in the three reactors, with average values around 36 and 0.5 mol L^{-1} , respectively (data not shown).

Dissolved oxygen and pH—Dissolved oxygen was never detected in the effluent (data not shown), indicating that microaerobic (i.e., $<4 \text{ } \mu\text{mol L}^{-1}$) or anaerobic conditions were achieved in the reactors. The pH showed an obvious decrease before day 63 (Fig. 2b), which can be attributed to production of protons during aerobic respiration. In turn, the pH increased between days 63 and 150, probably in response to manganese oxides, iron oxides, and sulfate reduction. It remained constant at pH 8.7 until the end of the experiment.

Metal reduction—Manganese reduction appeared to be the dominant redox process under microaerobic conditions between 0 and 12 d, with a maximum concentration of $84 \pm 16 \text{ } \mu\text{mol L}^{-1}$ on day 2, and declined sharply between 12 and 55 d to a minimum of $0.8 \pm 0.2 \text{ } \mu\text{mol L}^{-1}$ on day 55 (Fig. 3a). The total dissolved manganese concentration remained low during the rest of the experiment. Ferrous Fe, probably present in the residual pore waters, was initially flushed out of the reactors and by day 5 decreased to nondetectable values (Fig. 3b). It remained negligible until day 51 when it reappeared to reach a maximum concentration of $\sim 350 \text{ } \mu\text{mol L}^{-1}$ on day 67, as revealed by both the colorimetric and voltammetric methods.

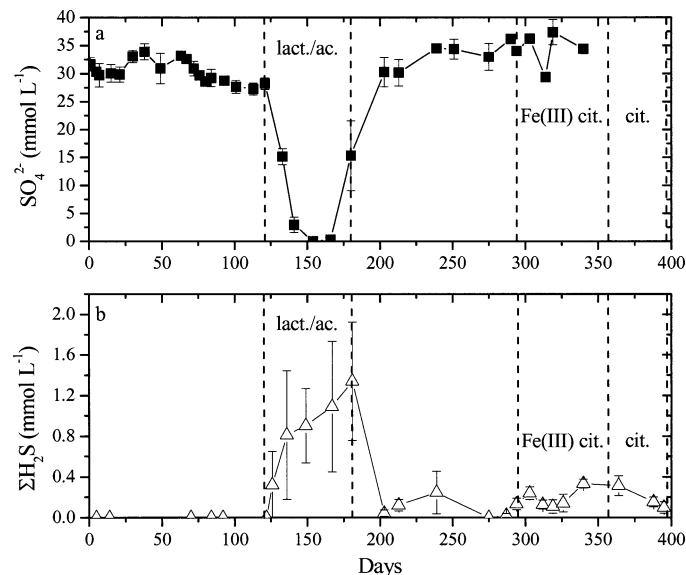


Fig. 4. (a) Average SO_4^{2-} and (b) $\Sigma\text{H}_2\text{S}$ concentrations as a function of time in the three reactors. The standard deviations represent the variations between the reactors. The days corresponding to the injection of the lactate/acetate mixture, ferric citrate, and sodium citrate are provided for reference.

metric and voltammetric methods. Total dissolved iron concentrations (Fe_d) indicate that iron was essentially in the form of Fe^{2+} in all three reactors (Fig. 3b). Interestingly, relatively large current intensities of soluble organic $\text{Fe}^{(III)}$ detected by voltammetry were produced simultaneously with Fe^{2+} . These data suggest that the sensitivity of soluble organic $\text{Fe}^{(III)}$ at the voltammetric electrode was extremely high. Iron reduction decreased between day 67 and day 120 to minimum average Fe^{2+} concentrations in the three reactors of $62 \pm 49 \text{ } \mu\text{mol L}^{-1}$. Again, the total dissolved iron measurements indicate that pore water iron was mainly in its reduced form. The voltammetric signals for Fe^{2+} and soluble organic $\text{Fe}^{(III)}$ followed a similar decrease during this period of time.

The initial response of the sediment to the addition of the lactate/acetate mixture on day 120 was a rapid increase in iron reduction (inset in Fig. 3b), with maximum concentrations of Fe^{2+} and Fe_d in the three reactors of 116 ± 9 and $139 \pm 21 \text{ } \mu\text{mol L}^{-1}$, respectively. This spike in Fe^{2+} was then followed by an equally abrupt decrease to nondetectable values for the duration of the experiment. Overall it is apparent from Fig. 3b that the conditions most suitable for iron reduction were found in the microaerobic and suboxic regimes.

Sulfate reduction—Sulfate was injected at a constant concentration of 28 mmol L^{-1} in the three reactors but was not consumed significantly before introduction of the lactate/acetate mixture on day 120 (Fig. 4a). Neither bisulfide and dissolved elemental sulfur (i.e., $\Sigma\text{H}_2\text{S} < 0.2 \text{ } \mu\text{mol L}^{-1}$) nor aqueous FeS were detected between days 51 and 120. Injection of the organic mixture resulted in the rapid and almost instantaneous reduction of SO_4^{2-} and subsequent production of $\Sigma\text{H}_2\text{S}$, with a maximum concentration of $1.3 \pm 0.6 \text{ mmol}$

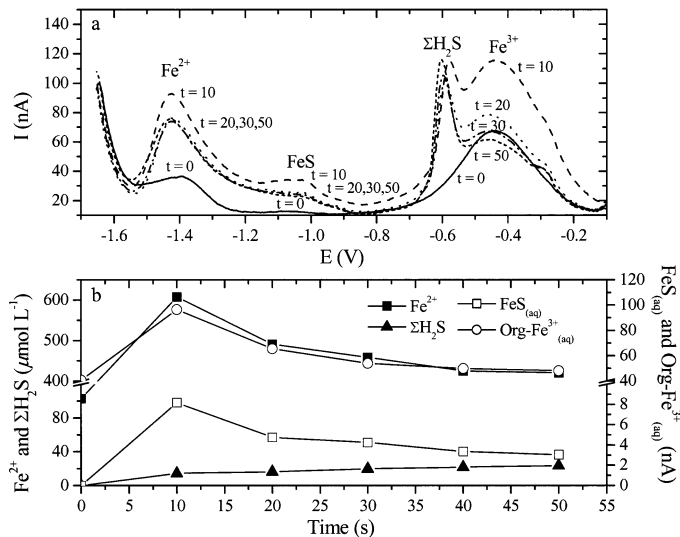


Fig. 5. Reduction of $500 \mu\text{mol L}^{-1}$ ferric citrate by $20 \mu\text{mol L}^{-1}$ $\Sigma\text{H}_2\text{S}$ as a function of time. (a) Time evolution of cathodic square wave voltammograms as a function of time. (b) Time evolution of Fe^{2+} and $\Sigma\text{H}_2\text{S}$ concentrations and $\text{FeS}_{(\text{aq})}$ and soluble organic $\text{Fe}^{(\text{III})}$ current intensities. The $\Sigma\text{H}_2\text{S}$ and soluble organic $\text{Fe}^{(\text{III})}$ peaks were deconvoluted with PeakFit.

L^{-1} between the three reactors (Fig. 4b). Interestingly, only $\sim 5\%$ of the SO_4^{2-} lost in the reactors was found as $\Sigma\text{H}_2\text{S}$, which suggests removal of sulfur from the pore waters by another mechanism. Although lactate was discontinued from the feeding solution after day 174, sulfate reduction, as measured by $\Sigma\text{H}_2\text{S}$ concentration, ensued and did not completely subside until day 275 (Fig. 4b).

The role of soluble organic $\text{Fe}^{(\text{III})}$ on iron and sulfur cycling—Fifteen days after the disappearance of dissolved sulfide from the effluents (day 290), ferric citrate was introduced into the reactors. Ferric citrate was chosen as a proxy for the soluble organic $\text{Fe}^{(\text{III})}$ complexes detected in sediment pore waters by voltammetry because it contains an organic moiety that is not metabolized by metal or sulfate-reducing bacteria and provides a voltammetric signal similar to that of pore water-soluble organic $\text{Fe}^{(\text{III})}$.

Ferric citrate was probably reduced and removed from the pore waters because no Fe^{2+} , soluble organic $\text{Fe}^{(\text{III})}$, or $\text{FeS}_{(\text{aq})}$ was detected in the effluent of the three reactors (Fig. 3b). In addition, the input of ferric citrate resulted in an increase in sulfate reduction, with production of up to $334 \pm 44 \mu\text{mol L}^{-1}$ $\Sigma\text{H}_2\text{S}$ on day 340 in the three reactors (Fig. 4b). The $\Sigma\text{H}_2\text{S}$ concentration remained constant until ferric citrate was replaced with a solution of sodium citrate on day 379. The sulfide concentration then rapidly decreased to a concentration of $154 \pm 47 \mu\text{mol L}^{-1}$ by day 388 and $98 \pm 57 \mu\text{mol L}^{-1}$ on day 395 (Fig. 4b). These data suggest that the soluble organic $\text{Fe}^{(\text{III})}$ complexes must have been reduced very quickly to Fe^{2+} and subsequently precipitated as FeS , pyrite, or both in the presence of dissolved sulfide produced by sulfate reduction.

This hypothesis was tested in a controlled experiment by reacting ferric citrate with H_2S . The experiment confirmed

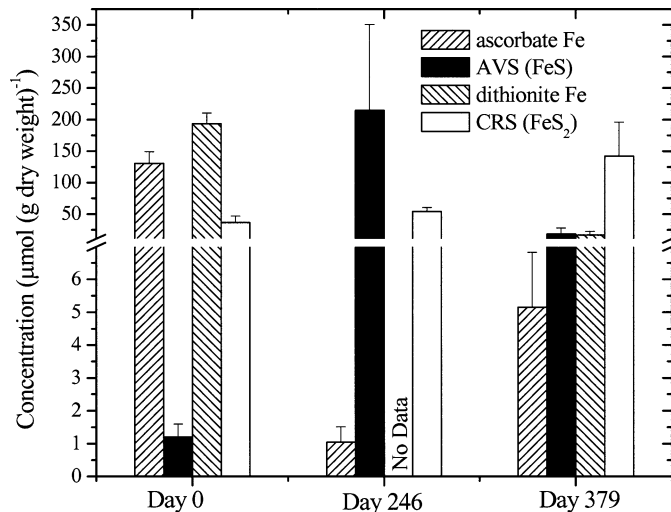


Fig. 6. Average ascorbate Fe ($\mu\text{mol Fe g}^{-1}$ dry sediment), AVS ($\mu\text{mol S g}^{-1}$ dry sediment), dithionite Fe ($\mu\text{mol Fe g}^{-1}$ dry sediment), and CRS ($\mu\text{mol S g}^{-1}$ dry sediment) extractions as a function of time. The standard deviation reflects the variation from the mean of three reactors, except in the case of the bulk sediment (day 0), for which it represents the variation of triplicate measurements. Note the break in the y-axis.

that the reduction of ferric citrate by H_2S is quasi-instantaneous (Fig. 5) and results in the simultaneous formation of $\text{FeS}_{(\text{aq})}$. The $\text{FeS}_{(\text{aq})}$ signal decreased after a few seconds, probably because of the rapid precipitation of $\text{FeS}_{(\text{s})}$, consistent with the increasingly black color of the solution. This experiment confirms that the reduction of ferric citrate in the presence of dissolved sulfide is extremely fast and suggests that all the ferric citrate in the reactors was removed as solid FeS , pyrite, or both.

Composition of iron and sulfur in the sediment—The initial bulk sediment was characterized by high ascorbate Fe with an average concentration of $131 \pm 19 \mu\text{mol Fe g}^{-1}$ and even higher dithionite Fe with an average concentration of $194 \pm 17 \mu\text{mol Fe g}^{-1}$ (Fig. 6). The FeS_2 and AVS were significantly lower in the bulk sediment, with average concentrations of $37 \pm 10 \mu\text{mol S g}^{-1}$ and $1.2 \pm 0.4 \mu\text{mol S g}^{-1}$, respectively. Crystalline Fe is defined as the difference between dithionite Fe and the sum of ascorbate Fe and AVS. The calculated crystalline Fe fraction in the bulk sediment was $\sim 62 \mu\text{mol Fe g}^{-1}$, indicating that, overall, the crystalline Fe oxide content in the reactors was much less than the concentration of amorphous iron oxides.

On day 246, ascorbate Fe was drastically lower in the three reactors, with an average concentration of $1 \pm 0.5 \mu\text{mol Fe g}^{-1}$ (Fig. 6). Relative to the decrease in ascorbate Fe, AVS showed a corresponding increase in concentration in all three reactors to an average of $215 \pm 136 \mu\text{mol S g}^{-1}$. Interestingly, on day 246, AVS yielded concentrations greater than the initial concentration of amorphous iron oxides in the bulk sediment, suggesting that reduction of less reactive, more crystalline iron oxides provided some of the reduced iron in the solid phase. The pyrite content of the three re-

actors increased slightly to an average concentration of $54 \pm 6 \mu\text{mol S g}^{-1}$.

On day 379, ascorbate Fe, although still low, increased slightly in all three reactors to reach a final average concentration of $5.2 \pm 1.7 \mu\text{mol Fe g}^{-1}$ (Fig. 6). Dithionite Fe showed a marked decrease over the course of the year, reaching a final average concentration of $17 \pm 5.6 \mu\text{mol Fe g}^{-1}$. From these data, crystalline Fe appears to have been totally consumed over the course of the experiment. AVS showed an unexpected decrease from day 246 to a final average concentration of $18 \pm 9.5 \mu\text{mol S g}^{-1}$ on day 379. However, the decrease in AVS was accompanied by an increase in pyrite to a final average concentration for the three reactors of $143 \pm 54 \mu\text{mol S g}^{-1}$.

Discussion

Plug-flow reactors (PFRs) may help characterize biogeochemical reactions in sediments (Roychoudhury et al. 1998, 2003) because they are relatively easy to use and minimize the perturbation of complex microbial assemblages that are inevitable in slurry or culture experiments. PFRs also provide a means to manipulate the pore-water composition over time to observe its effect on microbial and geochemical processes in sediments. In this study, manipulations were performed to investigate the role of soluble organic Fe(III) on the transformation of iron sulfur minerals in salt marsh sediments.

Transport parameters and reaction rates—Fluid velocity within the PFRs was kept slow and constant to avoid channelization, which could largely influence the biogeochemical reactions occurring within the sediment (Roychoudhury et al. 1998). Breakthrough curves for the bromide tracer (Fig. 2a) were used with a transient one-dimensional advection–dispersion model (Eq. 5) to determine the dispersion coefficient (D), the advection rate (v), and the retardation factor (R) within the reactors (Roychoudhury et al. 1998).

$$R \frac{dC}{dt} = D \frac{\partial^2 C}{\partial x^2} - v \frac{\partial C}{\partial x} \quad (5)$$

The analytical solution to the governing equation (Van Genuchten 1981) was used with an optimization procedure to calculate the three parameters. The optimization procedure, written in Matlab[®], minimizes, in a least-squares fashion, the difference between the data and the analytical solution of the differential equation to determine the three unknown parameters. The boundary conditions consistent with a PFR are as in Eq. 6,

$$C(x, 0) = 0 \quad C(0, t) = C_0 \quad \frac{\partial}{\partial x} C(L, t) = 0 \quad (6)$$

where x is the spatial variable in the reactor, t is time, L is the total length of the sediment plug, and C_0 is the input concentration of bromide.

The tracer test was applied at two different occasions during the experiment (Fig. 2a) to determine whether the hydraulic parameters had changed over time. The modeled average bromide concentrations fit the data well (Fig. 2a), and

the model, not surprisingly, shows that retardation is minimal and diffusion dispersive. Interestingly, the model provides similar retardation factors and dispersion coefficients for both breakthrough curves, but the advection coefficient calculated after day 136 is ~ 10 times lower than in the first part of the experiment. These findings suggest that the porosity of the sediment decreased over time and are consistent with the changes in sediment morphology resulting from FeS precipitation (Fig. 6).

Net reaction rates were calculated with a modified version of the transient one-dimensional advection–dispersion model that included a reaction rate term at the end of Eq. 5. The production or consumption rates were determined for time periods during which some of the species of interest were constantly injected into the reactors and chemical changes were observed in the effluents of the reactors. As a consequence, the boundary conditions differed slightly from Eq. 6 to include a flux-type boundary at the inlet of the reactors,

$$C(x, t_0) = C_0 \quad -D \frac{\partial C}{\partial x} + vC|_{x=0} = vC_0 \quad \frac{\partial}{\partial x} C(L, t) = 0 \quad (7)$$

where $t_0 \geq 0$ is the initial time selected to determine rates during a particular time period and all the other parameters are the same as before. The analytical solution to the governing equation (Van Genuchten 1981) and the transport parameters calculated from the bromide breakthrough curves were used to determine the net reaction rates by fitting the data from the reactors' effluents over time by least-squares optimization as described previously.

Metal reduction—The first 5 d of the experiment were marked by the flushing of high concentrations of Mn^{2+} and Fe^{2+} (Fig. 3), probably produced by microbial manganese and iron reduction (Kostka and Luther 1995; Kostka et al. 2002; Koretsky et al. 2003) or chemical reduction of manganese oxides by Fe^{2+} (Postma 1985) before the beginning of the experiment.

Table 1 tabulates the net production and consumption rates of total dissolved Mn, Fe^{2+} by ferrozine and voltammetry, SO_4^{2-} , and $\Sigma\text{H}_2\text{S}$ in the PFRs beginning after 5 d (Figs. 3, 4). This sediment was characterized by iron reduction in the suboxic regime but, surprisingly, little manganese reduction. From the data, it is not clear whether the absence of Mn^{2+} after 27 d was the result of a decrease in manganese reduction, a removal of Mn^{2+} by adsorption (Van Cappellen and Wang 1996), or simply a low content of manganese oxides in these sediments. The rates of Fe^{2+} production and consumption determined by voltammetry and ferrozine are comparable between days 34 and 120 (Table 1), which indicates that voltammetric measurements with Au/Hg microelectrodes in marine sediments can be trusted.

Soluble organic Fe^{III} , detected simultaneously with the production of Fe^{2+} between days 34 and 95, could be an intermediate in the reduction of iron oxides. At the pH of these incubations, iron oxides can be reduced either chemically by dissolved sulfide or microbially. The mechanism of iron oxide reduction by dissolved sulfide first involves adsorption of bisulfide on the oxide surface then reduction of

Table 1. Net reaction rates for dissolved Mn, Fe²⁺ (ferrozine and voltammetry), SO₄²⁻, and ΣH₂S over the course of the experiment. The reaction rates represent the average change in concentration as a function of time and the standard deviation for each set of measurements. Days were separated on the basis of changing redox conditions during the incubations. Positive and negative rates indicate production and consumption of a species, respectively. A dash indicates that the reaction rate could not be calculated.

	Days	Mn _d (μmol L ⁻¹ d ⁻¹)	Ferrozine Fe ²⁺ (μmol L ⁻¹ d ⁻¹)	Voltammetry Fe ²⁺ (μmol L ⁻¹ d ⁻¹)	SO ₄ ²⁻ (μmol L ⁻¹ d ⁻¹)	ΣH ₂ S (μmol L ⁻¹ d ⁻¹)
μ-Aerobic	5–40	-0.017 ± 0.011	0	0	0	0
	34–67	0	28.8 ± 2.8	37.3 ± 10.3	0	0
Suboxic	67–120	0	-4.5 ± 0.7	-66.6 ± 3.0	-364 ± 61	0
	121–125	0	13.6 ± 9.7	—	—	0
Anoxic	125–174	0	-15.5 ± 1.4	—	-727 ± 67	28.8 ± 4.7
	174–290	0	0	0	—	-50.5 ± 13.4
	290–366	0	0	0	—	4.75 ± 0.1
	366–396	0	0	0	—	-5.59 ± 2.1

ferric iron to ferrous iron, followed by the departure of ferrous iron from the surface (Pyzik and Sommers 1981; Peiffer et al. 1992; Yao and Millero, 1996). Therefore, it is unlikely that sulfide is involved in the production of soluble organic Fe^(III). In addition, soluble organic Fe^(III) is readily reduced by dissolved sulfide to produce S⁰ and FeS_(aq) (Fig. 5; Taillefert et al. 2000). The increase in soluble organic Fe^(III) between days 34 and 70, the absence of H₂S, S⁰, and FeS_(aq), the constant SO₄²⁻ concentration (Fig. 4), and the dominance of Fe²⁺ in the effluent seawater (Fig. 3b) all suggest that microbial reduction of iron oxides within the sediment was the main process of iron reduction between days 34 and 67. Because both microbial iron reduction and reduction of iron oxides by sulfide (without precipitation of FeS) result in an increase in pH, the concomitant pH and Fe²⁺ increases in the reactors during that time period (Figs. 2b, 3b) cannot help to differentiate these processes. Altogether, these data suggest that soluble ferric iron complexes could be intermediates in the bacterial reduction of iron oxides. Indeed, it has been shown that exogenous organic ligands nonreductively dissolve iron oxides to produce soluble organic Fe^(III) complexes (Luther et al. 1992), which are more readily reduced by microorganisms (Arnold et al. 1988; Lovley and Woodward 1996; Dollhopf et al. 2000). In addition, some iron-reducing bacteria generate relatively high concentrations of soluble Fe(III) in the absence of exogenous ligands (Nevin and Lovley 2002), an indication that these bacteria synthesize and release endogenous chelators to solubilize Fe(III) before reduction.

Sulfate reduction and precipitation of FeS and FeS₂—Between days 67 and 120, the average sulfate reduction rate

Table 2. Reaction rates for the transformation of amorphous iron oxides, FeS, and pyrite calculated from the solid phase extractions of Fig. 6, assuming a sediment density of 0.78 g cm⁻³. Positive and negative rates indicate production and consumption of a species, respectively.

Days	Ascorbate Fe (μmol L ⁻¹ d ⁻¹)	AVS (FeS) (μmol L ⁻¹ d ⁻¹)	Pyrite (FeS ₂) (μmol L ⁻¹ d ⁻¹)
0–246	-411	678	27.6
246–379	24.1	-1153	259

for the three reactors was on the order of 360 μmol L⁻¹ d⁻¹. In turn, the net decrease in ferrous Fe concentration within the same time interval was on the order of 5 μmol L⁻¹ d⁻¹ (Table 1). The advent of sulfate reduction was not corroborated by detection of H₂S; however, the concomitant decrease in Fe²⁺ and SO₄²⁻ between days 67 and 120 (Figs. 3b, 4a) and the significantly higher sulfate reduction rate than iron reduction rate (Table 1) provide indirect evidence for chemical reduction of amorphous iron oxides by dissolved sulfide and for FeS (but not FeS₂) formation during that period of time (Fig. 6). If dissolved sulfide and pyrite are not produced, the rate of sulfate reduction must be equivalent to the rate of FeS precipitation. In turn, the rate of FeS precipitation is equivalent to the total loss of iron from the pore waters and the solid phase. From Table 1, we calculate a rate of iron oxide reduction by dissolved sulfide on the order of 360 μmol Fe L⁻¹ d⁻¹ between days 67 and 120, which corresponds to ~85% of the amorphous iron oxide reduction rate in the reactors during the first 250 d (Table 2).

A lactate/acetate mixture was injected into the reactors to provide dissolved organic metabolites such as those produced by salt marsh plants (e.g., *Spartina alterniflora*). Lactate/acetate mixtures have been used previously in the cultivation of iron-reducing (Arnold et al. 1988; Lowe et al. 2000) and sulfate-reducing (Lowe et al. 2000; Sass et al. 2002; Koretsky et al. 2003) bacteria. The initial response to the lactate/acetate mixture introduction into the PFRs was a sharp increase in Fe²⁺ (inset of Fig. 3b) at a rate of ~14 μmol Fe L⁻¹ d⁻¹ between days 121 and 125, followed by an equally sharp removal of Fe²⁺ (Table 1). The production of Fe²⁺ between days 121 and 125 could be a result of either microbial iron reduction or chemical reduction of iron oxides by dissolved sulfide (Yao and Millero 1996). Interestingly, our data did not display aqueous FeS, generally observed during the chemical reduction of iron oxides or soluble Fe(III) by dissolved sulfide (Fig. 5; Taillefert et al. 2000). After 125 d, sulfate reduction dominated and resulted in the total depletion of Fe²⁺ from the effluent seawater because of the rapid precipitation of FeS.

Sulfate concentrations decreased to nondetectable values in ~30 d during lactate injection, resulting in a maximum loss of ~28 mmol L⁻¹ SO₄²⁻, whereas dissolved sulfide in solution reached a maximum concentration of 1.3 mmol L⁻¹

only. This difference suggests that the remaining 27 mmol L⁻¹ of dissolved sulfide was used to reduce iron oxides and precipitate FeS. Indeed, the effluent seawater produced a bright yellow precipitate on injection of lactate that steadily lessened over the course of the 54 d of lactate injection. The yellow color is attributed to the formation of elemental sulfur (S₈) during the reduction of iron oxides by dissolved sulfide (Pyzik and Sommers 1981; Peiffer et al. 1992; Yao and Millero 1996), which could contribute to some of the voltammetric ΣH₂S detected at the output of the reactors (Fig. 4b). The formation of Fe²⁺ and subsequent precipitation of FeS through reduction of iron oxides by HS⁻ can also occur with production of polysulfides (S_x²⁻), thiosulfate (S₂O₃²⁻), and SO₄²⁻ (Peiffer et al. 1992). However, S₂O₃²⁻ was never detected by voltammetry, and background SO₄²⁻ concentrations were too high to observe its authigenic formation through this process. Only S_x²⁻ might have existed and contributed to the voltammetric ΣH₂S detected in the reactors (Fig. 4b).

Acid volatile sulfides measured on day 246 yielded 215 ± 136 μmol S g⁻¹, corresponding to 168 ± 106 mmol L⁻¹ FeS produced when considering an average sediment density of 0.78 g cm⁻³ (Gribsholt et al. 2003). Simultaneously, the average concentration of FeS₂ measured after 246 d was not significantly different from the bulk sediment composition at the beginning of the experiment (Fig. 6) and fell in the range of pyrite concentrations found at the surface of salt marsh sediments (Lord and Church 1983; King et al. 1985; Luther and Church 1988; Luther et al. 1992; Taillefert et al. 2002a). As a result, pyritization rates were not significant during lactate injection (Table 2), even though dissolved sulfide (Fig. 4b) and FeS (Fig. 6) were present in high concentrations in these sediments.

The rate of precipitation of FeS was much higher than the rate of reduction of amorphous iron oxides during the first 250 d (Table 2), which indicates that crystalline and amorphous iron oxides were both reduced and precipitated as FeS. To determine when FeS was precipitated during the incubations, we calculated the time evolution of FeS precipitation with a mass balance approach. For this calculation, the difference between the initial input SO₄²⁻ concentration and the sum of the concentration of SO₄²⁻ and ΣH₂S at each time step until day 250 was attributed to FeS because pyrite formation was not significant up to this point (*see* Fig. 6). The summed average concentration of FeS determined from this calculation (Fig. 7) and the solid phase extraction were in close agreement, 136 mmol L⁻¹ and 168 mmol L⁻¹, respectively. On the basis of these calculations, ~91% of the FeS precipitated in response to the injection of the lactate. These results are supported by the good correlation between the sulfate reduction rate determined between days 125 and 174 (727 ± 67 μmol S L⁻¹ d⁻¹; Table 1) and the rate of formation of FeS measured (678 μmol S L⁻¹ d⁻¹; Table 2). These data also indicate that the decrease in Fe²⁺ after day 67 was due to the production of dissolved sulfide by sulfate reduction.

The role of soluble organic Fe^(III) in FeS and FeS₂ precipitation—Ferric citrate was introduced into the reactors to determine the role of soluble organic Fe^(III) on the biogeochemical cycling of iron and sulfur in sediments. Pyrite precipitation was not significant during the first 246 d of the

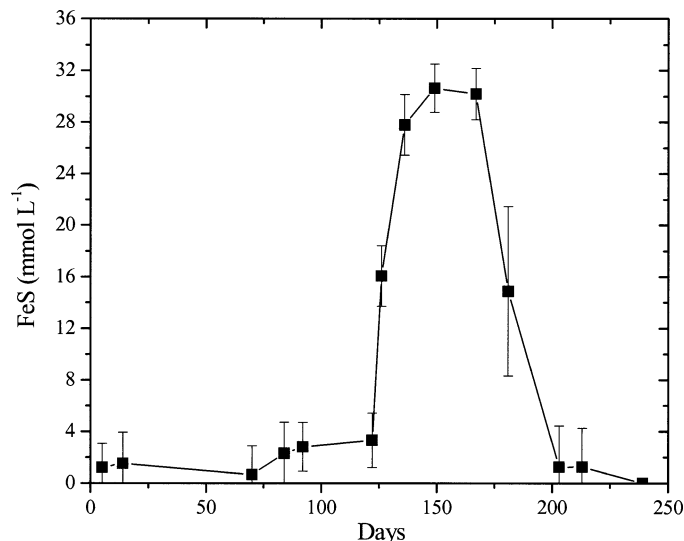


Fig. 7. FeS precipitation calculated from the difference between the input SO₄²⁻ and the resultant H₂S as a function of time up to day 250. Error bars denote the average and standard deviation for the three reactors.

experiment (Fig. 6). In contrast, pyrite tripled (Fig. 6), and the pyritization rate increased by an order of magnitude (Table 2) when ferric citrate was injected into the reactors. Interestingly, no Fe²⁺ was ever detected in the effluent, even with the injection of a total of 3 mmol ferric citrate during this period of time, but dissolved sulfide reappeared, suggesting that sulfate reduction was promoted by ferric citrate. It is well known from the microbiological literature that sulfate-reducing bacteria oxidize H₂ to reduce SO₄²⁻ (Lengeler et al. 1999). Sulfate-reducing bacteria generally obtain H₂ from the outside environment via complex microbial interactions or from the degradation of small organic ligands such as lactate and pyruvate (Lengeler et al. 1999). Thus, two mechanisms could have induced sulfate reduction on addition of ferric citrate. First, ferric citrate could have been degraded during fermentation processes to eventually produce molecular hydrogen (H₂) as the electron donor for sulfate-reducing bacteria. Second, H₂ could have been produced in sufficient quantities by other microbial processes to sustain sulfate reduction.

Because the dissolved sulfide concentration was still high during this time interval (Fig. 4), the chemical reduction of ferric citrate must have resulted in the precipitation of FeS or pyrite (Yao and Millero 1996; Taillefert et al. 2000, 2002a). Indeed, H₂S-mediated reduction of ferric citrate occurred on the order of seconds to minutes (Fig. 5). However, a pronounced decrease in the concentration of AVS was observed concomitantly with an increase in the concentration of pyrite over this duration (Fig. 6), suggesting that ferric citrate was reduced to form pyrite. Pyritization can arguably occur through a variety of processes involving elemental sulfur (S₈), polysulfides (S_x²⁻), H₂S, or even Fe²⁺ (Rickard 1975; Berner 1984; Luther 1991; Schoonen and Barnes 1991; Rickard and Luther 1997). However, precipitation through reaction of FeS with S_x²⁻ (Rickard 1975; Luther 1991) or

H₂S via the Wächterhauser mechanism (Rickard 1997) seems to be equally fast depending on pH.

To determine the pyritization rate in the presence of polysulfides (Eq. 3) formed in situ by the reaction of elemental sulfur (S₈) with dissolved sulfide, we used the rate law of Rickard (1975),

$$\frac{d}{dt}[\text{FeS}_2] = kA_{\text{FeS}}^2A_{\text{S}_8}\{\Sigma\text{H}_2\text{S}\}\{\text{H}^+\} \quad (8)$$

where $k = 1.5 \times 10^{-13} \text{ mol L}^{-1} \text{ cm}^{-6} \text{ s}^{-1}$ at 25°C is the rate constant (Rickard 1975), A_{FeS} and A_{S_8} are the surface areas of FeS and S₈, respectively. The surface area of FeS was estimated from the average maximum concentration of FeS measured at day 246 and a specific surface area of $1.6 \times 10^5 \text{ cm}^2 \text{ g}^{-1}$ (Rickard 1975). The concentration of S₈ was estimated assuming that all the ferric citrate was reduced by dissolved sulfide and produced S₈ as a result of the oxidation of dissolved sulfide. This concentration and a specific surface area of $1.4 \times 10^3 \text{ cm}^2 \text{ g}^{-1}$ (Rickard 1975) were used to calculate the surface area of S₈. The activities of the dissolved sulfide species were calculated from the concentration of total dissolved sulfide and the pH measured between days 246 and 395 (Figs. 2b, 4b) and the acid–base equilibrium of H₂S. The first acid–base equilibrium constant and the activity coefficients were obtained from Millero (1986).

The rates obtained range between 1.29 ± 0.12 and $10.2 \pm 0.9 \text{ nmol L}^{-1} \text{ d}^{-1}$ depending on the concentration of total dissolved sulfide (0.17 ± 0.09 and $1.34 \pm 0.6 \text{ mmol L}^{-1}$) used for this calculation. These rates are much lower than found in typical coastal sediments (Luther 1991) and measured in this study (Table 2). Even though it is possible that our assumption of the concentration of elemental sulfur is wrong, the calculated surface area of S₈ is close to that determined by Rickard (1975) and should not affect the rates significantly. In turn, it is likely that polysulfides formed in our experiment were more reactive than those formed in the presence of crystalline S₈ because elemental sulfur in our experiments was probably a soluble or colloidal product of the reaction of ferric citrate with dissolved sulfide, which can react very rapidly. Similarly, it is possible that the specific surface area of FeS is much higher when formed through reduction of ferric citrate by dissolved sulfide. It is therefore less likely that the rate law of Eq. 8 can be used to accurately predict the pyritization rate in our incubations.

To determine whether pyrite formation between days 246 and 395 followed Wächterhauser's mechanism (Eq. 2), pyritization rates were calculated from the rate law of Rickard (1997),

$$\frac{d}{dt}[\text{FeS}_2] = k[\text{FeS}][\text{H}_2\text{S}] \quad (9)$$

where [FeS] is the maximum concentration for the three reactors measured at day 246 (Fig. 6) and $k (1.03 \times 10^{-4} \text{ L mol}^{-1} \text{ s}^{-1}$ at 25°C) is the rate constant provided by Rickard (1997). The concentration of hydrogen sulfide and the pH were obtained as mentioned previously.

Rickard (1997) found that the rate of pyrite formation is strongly dependent on FeS but inversely correlated to pH because the molecular orbitals of sulfur in HS⁻ are not fa-

vorably oriented to react with the S⁰ of pyrite compared with those of H₂S (Rickard and Luther 1997). The rates obtained with the Wächterhauser mechanism range between 2.83 ± 0.6 and $22.3 \pm 3.1 \text{ } \mu\text{mol L}^{-1} \text{ FeS}_2 \text{ d}^{-1}$ depending on the concentration of total dissolved sulfide (0.17 ± 0.09 and $1.34 \pm 0.6 \text{ mmol L}^{-1}$) used for this calculation. These rates are significantly faster than those made available by Rickard (1997) in typical sulfidic sediments at ambient temperature (9×10^{-7} to $0.09 \text{ } \mu\text{mol L}^{-1} \text{ FeS}_2 \text{ d}^{-1}$). However, they are not as fast as those measured directly (Table 2), suggesting that ferric citrate accelerates the formation of pyrite to levels well beyond those previously observed in other systems. Donald and Southam (1999) observed bacterially catalyzed pyritization at the surface of sulfate-reducing bacteria and proposed that the cells act as a nucleation center for FeS formation and pyrite precipitation with bacterially released H₂S. Such bacterial catalysis could be involved in the fast pyritization observed in our experiments. However, at the pH of these incubations, the reaction with polysulfides is most likely the main mechanism of FeS₂ formation in these sediments (Luther 1991). Therefore, we propose that the fast chemical reduction of ferric citrate by dissolved sulfide produces a soluble or colloidal elemental sulfur that can react further with bisulfide to form a very reactive soluble or colloidal S_x²⁻ to catalyze the formation of pyrite in the presence of amorphous FeS. At this point, it is not sure whether bacteria catalyze this reaction, but the rate law and the rate constant proposed by Rickard (1975) cannot describe this mechanism.

Altogether, the data collected in this study suggest that soluble organic Fe^(III) is produced as an intermediate (pathway 1 in Fig. 8) in the reduction of iron oxides (pathway 2 and 3 in Fig. 8), the mechanism of formation of soluble organic Fe^(III) in suboxic conditions is still unclear: iron oxides could be nonreductively dissolved by organic ligands (Luther et al. 1992) to form electrochemically labile complexes. Alternatively, iron-reducing bacteria could generate soluble organic Fe^(III) with the use of an endogenous organic ligand to solubilize iron oxides before reduction (Nevin and Lovley 2002). In both cases, iron-reducing bacteria could benefit from the formation of these complexes by transferring electrons to a more reactive soluble ferric iron (pathway 2 in Fig. 8; Arnold et al. 1988; Lovley and Woodward 1996; Dollhopf et al. 2000). In anoxic conditions, when sulfate reduction is active in the presence of small organic electron donors (pathway 4 in Fig. 8), the chemical reduction of iron oxides via surface interaction with sulfide species (Pyzik and Sommer 1981; Peiffer et al. 1992; Yao and Millero 1996) results in the production of S₈ (pathway 3 in Fig. 8) and FeS_(s) (pathway 5 in Fig. 8), possibly with FeS_(aq) as an intermediate (Rickard 1995). Interestingly, our data indicate that in the presence of low soluble Fe(III) concentration, the reduction of iron oxides results in the formation of FeS_(s), only without the occurrence of an FeS_(aq) intermediate and without production of pyrite. However, in the presence of a high concentration of soluble Fe(III), sulfate reduction is activated, possibly through complex bacterial interactions involving fermentation processes, and the formation of pyrite (pathway 6 and 7 in Fig. 8), rather than its oxidation, is catalyzed. The mechanism of pyrite formation should de-

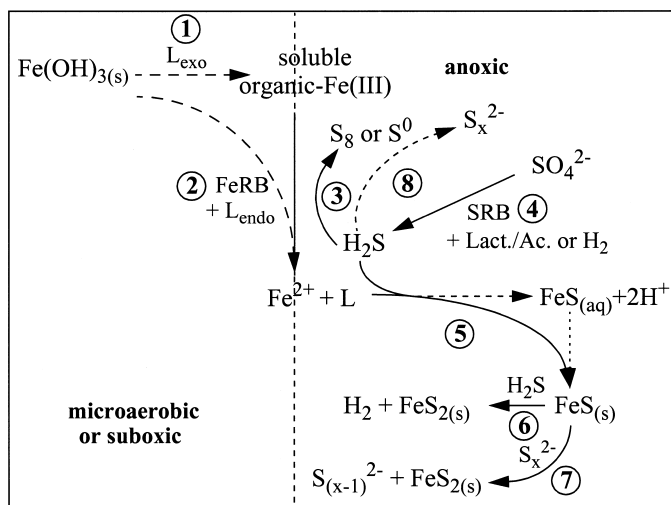


Fig. 8. Schematic diagram of iron and sulfur cycling at the redox interface in salt marsh sediments as revealed by the incubations. Dashed lines represent hypothesized or proposed processes. In microaerobic and suboxic conditions, soluble organic Fe^(III) can be produced as an intermediate in the reduction of iron oxides, either chemically in the presence of exogenous organic ligands (pathway 1) or directly by iron-reducing bacteria via endogenous ligands (pathway 2). In anoxic conditions, sulfate reduction produces dissolved sulfide in the presence of exogenous H₂ or small organic ligands (pathway 4). Dissolved sulfide then reduces soluble organic Fe^(III) and iron oxides to produce Fe²⁺ and, respectively, S⁰ or S₈ (pathway 3). Subsequently, FeS precipitates, possibly through the formation of an intermediate FeS_(aq) cluster (pathway 5). Pyritization is accelerated in the presence of soluble organic Fe^(III) and proceeds by reaction of FeS_(s) with H₂S (pathway 6) and polysulfides (pathway 7), although the former should be much less efficient at the pH of these sediments. Polysulfides are formed by the fast reaction of S⁰, produced during the reduction of soluble organic Fe^(III) by dissolved sulfide (pathway 8), with dissolved sulfide produced by sulfate-reducing bacteria (pathway 4). We propose that the polysulfides formed in the presence of soluble organic Fe^(III) are highly reactive and catalyze the formation of pyrite. Oxidation of pyrite is not observed in anoxic conditions, even in the presence of soluble organic Fe(III).

pend on the pH of the system (Luther 1991). At pH < 7, the Wächterhauser mechanism (pathway 6 in Fig. 8; Rickard 1997; Rickard and Luther 1997) should be favored, but at the high pH of our experiments, the formation of pyrite by reaction with polysulfides (pathway 7 in Fig. 8) should prevail. Our data indicate that soluble Fe(III) catalyzes the formation of pyrite with rates that cannot be described by existing rate laws (Rickard 1975, 1997). These findings suggest that the high reactivity of soluble organic Fe^(III) with dissolved sulfide could result in the formation of a highly reactive soluble elemental sulfur (S⁰) that could catalyze the production of polysulfides (pathway 8 in Fig. 8) if dissolved sulfide is in excess. These polysulfides could then react with FeS_(aq) or FeS_(s) much faster than estimated when polysulfides are formed from solid elemental sulfur. This process appears to be self-sustained as long as soluble organic Fe(III) is supplied to the sediments with an organic ligand that can be directly metabolized by sulfate-reducing bacteria or fermented to produce electron donors for sulfate-reducing bac-

teria. These data suggest that in anoxic coastal marine sediments, organic Fe^(III) complexes can promote the precipitation of FeS₂ by incidentally providing sulfate-reducing bacteria with the necessary chemicals (i.e., Fe or organic ligands). It is now imperative to determine the abundance and composition of these complexes in sediments to assess their importance on a global scale.

In summary, plug-flow reactors provide an excellent means for studying complex biogeochemical reaction mechanisms in sediments. They are easily maintained and can be manipulated to isolate specific biogeochemical processes. To accurately determine these processes, it is necessary to continuously monitor the chemistry of the effluent water as well as take intermittent solid phase measurements. Flow cells, complemented with electrochemical techniques, offer an innovative and practical way to obtain real-time data. In this study, small sediment PFRs were employed to investigate the cycling of Fe and sulfur in the first few centimeters of salt marsh sediment in an effort to better constrain the reaction mechanisms by which FeS and FeS₂ precipitate.

The data provided by the PFRs over the 13-month duration of the experiment cohesively describe the processes involved in the evolution from largely oxidized to dominantly reduced sediments. Taken together, the data seem to support previous work that shows the occurrence of microbial iron reduction in shallow salt marsh sediments. In the presence of highly metabolizable organic compounds such as lactate and acetate, sulfate reduction outcompetes iron reduction and results in the total depletion of Fe²⁺ from pore waters because of the rapid precipitation of FeS.

Surprisingly, sulfate reduction was promoted with the addition of ferric citrate as a proxy for soluble organic Fe^(III), suggesting that the organic moiety could have been fermented to produce readily metabolizable electron donors for sulfate-reducing bacteria. Although FeS precipitation should have been promoted in the presence of ferric citrate because the chemical reduction of soluble organic Fe^(III) by dissolved sulfide is extremely fast, pyritization was catalyzed by ferric citrate. Pyritization rates measured in these sediments are significantly faster than those determined previously in typical sulfidic sediments at ambient temperatures and cannot be explained by rate laws obtained in laboratory conditions with well-crystallized minerals. At the pH of these incubations, the reaction with polysulfides is most likely the main mechanism of FeS₂ formation in these sediments. We therefore propose that the chemical reduction of ferric citrate by dissolved sulfide produces a soluble or colloidal elemental sulfur that can react further with bisulfide to form a very reactive soluble or colloidal S_x²⁻ to catalyze the formation of pyrite.

These findings have important implications in diagenesis. First, soluble organic Fe^(III) seems to promote FeS₂ formation within shallow anoxic salt marsh sediments if dissolved sulfide is in excess. If iron is sequestered in FeS₂, the remineralization of NOM will mainly be achieved through sulfate reduction because SO₄²⁻ is not limiting in marine pore waters and because FeS₂ formation through soluble organic Fe^(III) could generate enough H₂ to sustain sulfate reduction. Microbial iron reduction will prevail only if dissolved O₂ is periodically supplied to the sediment. Dissolved O₂ will both

inhibit sulfate-reducing bacteria and oxidize Fe²⁺ very rapidly. In such conditions, the supply of freshly formed iron oxides will promote microbial iron reduction, and the sediment will remain suboxic. The origin and quantification of soluble organic Fe(III) need to be resolved to elucidate the exact role played by these complexes. Preliminary experiments with model iron-reducing bacteria indicate that they could be produced microbially as intermediate complexes during the reduction of iron oxides.

References

- ARNOLD, R. G., T. J. DICHRISTINA, AND M. R. HOFFMANN. 1988. Reductive dissolution of Fe(III) oxides by *Pseudomonas* sp. 200. *Biotechnol. Bioeng.* **32**: 1081–1096.
- BERNER, R. A. 1984. Sedimentary pyrite formation: An update. *Geochim. Cosmochim. Acta* **48**: 605–615.
- BRENDEL, P. J., AND G. W. LUTHER III. 1995. Development of a gold amalgam voltammetric microelectrode for the determination of dissolved Fe, Mn, O₂, and S(–II) in porewaters of marine and freshwater sediments. *Environ. Sci. Technol.* **29**: 751–761.
- BULL, D. C., AND M. TAILLEFERT. 2001. Seasonal and topographic variations in porewaters of a southeastern USA salt marsh as revealed by voltammetric profiling. *Geochem. Trans.* **13**: 1–8.
- CANFIELD, D. E., R. RAISWELL, J. T. WESTRICH, C. M. REAVES, AND R. A. BERNER. 1986. The use of chromium reduction in the analysis of reduced inorganic sulfur in sediments and shales. *Chem. Geol.* **54**: 149–155.
- DE VITRE, R., J. BUFFLE, D. PERRET, AND R. BAUDAT. 1988. A study of iron and manganese transformations at the O₂/S(–II) transition layer in a eutrophic lake. *Geochim. Cosmochim. Acta* **52**: 1601–1613.
- DICHRISTINA, T. J., C. M. MOORE, AND C. HALLER. 2002. Dissimilatory Fe(III) and Mn(IV) reduction by *Shewanella putrefaciens* requires ferE, a pulE (gspE) homolog of Type II protein secretion. *J. Bacteriol.* **184**: 142–151.
- DICKSON, A. G. 1993. pH buffers for seawater media based on the total hydrogen ion concentration scale. *Deep-Sea Res. I* **40**: 107–118.
- DOLLHOPF, M. E., K. H. NEALSON, D. M. SIMON, AND G. W. LUTHER III. 2000. Kinetics of Fe(III) and Mn(IV) reduction by the Black Sea strain of *Shewanella putrefaciens* using in situ solid state voltammetric Au/Hg electrodes. *Mar. Chem.* **70**: 171–180.
- DONALD, R., AND G. SOUTHAM. 1999. Low temperature anaerobic bacterial diagenesis of ferrous monosulfide to pyrite. *Geochim. Cosmochim. Acta* **63**: 2019–2023.
- GRIBSHOLT, B., J. E. KOSTKA, AND E. KRISTENSEN. 2003. Impact of fiddler crabs and plant roots on sediment biogeochemistry in a Georgia salt marsh. *Mar. Ecol. Prog. Ser.* **259**: 237–251.
- HAAS, J. R., AND T. J. DICHRISTINA. 2002. Effects of Fe(III) chemical speciation on dissimilatory Fe(III) reduction by *Shewanella putrefaciens*. *Environ. Sci. Technol.* **63**: 373–380.
- HENNEKE, E., G. W. LUTHER III, AND G. J. DE LANGE. 1991. Determination of inorganic sulphur speciation with polarographic techniques: Some preliminary results for recent hypersaline anoxic sediments. *Mar. Geol.* **100**: 115–123.
- HOWARTH, R. W. 1984. The ecological significance of sulfur in the energy dynamics of salt marsh and coastal marine sediments. *Biogeochemistry* **1**: 5–27.
- JACOBSEN, M. E. 1994. Chemical and biological mobilization of Fe(III) in marsh sediments. *Biogeochemistry* **25**: 41–60.
- JORGENSEN, B. B. 1982. Mineralization of organic matter in the sea bed—the role of sulfate reduction. *Nature* **296**: 643–645.
- KING, G. M., B. L. HOWES, AND J. W. H. DACEY. 1985. Short-term end-products of sulfate reduction in a salt-marsh—formation of acid volatile sulfides, elemental sulfur, and pyrite. *Geochim. Cosmochim. Acta* **49**: 1561–1566.
- KORETSKY, C. M., C. M. MOORE, K. L. LOWE, C. MEILE, T. J. DICHRISTINA, AND P. VAN CAPPELLEN. 2003. Seasonal oscillation in microbial iron and sulfate reduction in salt marsh sediments. *Biogeochemistry* **64**: 179–203.
- KOSTKA, J. E., B. GRIBSHOLT, E. PETRIE, D. DALTON, H. SKELTON, AND E. KRISTENSEN. 2002. The rates and pathways of carbon oxidation in bioturbated salt marsh sediments. *Limnol. Oceanogr.* **47**: 230–240.
- , AND G. W. LUTHER III. 1994. Partitioning and speciation of solid phase iron in salt marsh sediments. *Geochim. Cosmochim. Acta* **58**: 1701–1710.
- , AND G. W. LUTHER III. 1995. Seasonal cycling of Fe in salt marsh sediments. *Biogeochemistry* **29**: 159–181.
- LENGELER, J. W., G. DREWS, AND H. H. SCHLEGEL. 1999. *Biology of prokaryotes*. Blackwell Science.
- LORD, C. J. III, AND T. M. CHURCH. 1983. The geochemistry of salt marshes: sedimentary ion diffusion, sulfate reduction, and pyritization. *Geochim. Cosmochim. Acta* **47**: 1381–1391.
- LOVLEY, D. R., AND J. C. WOODWARD. 1996. Mechanisms for chelator simulation of microbial Fe(III)-oxide reduction. *Chem. Geol.* **132**: 19–24.
- LOWE, K. L., T. J. DICHRISTINA, A. N. ROYCHOUDHURY, AND P. VAN CAPPELLEN. 2000. Microbiological and geochemical characterization of microbial Fe(III) reduction in salt marsh sediments. *Geomicrobiol. J.* **17**: 163–178.
- LUTHER, G. W. III. 1991. Pyrite synthesis via polysulfide compounds. *Geochim. Cosmochim. Acta* **55**: 2839–2849.
- , A. B. BONO, M. TAILLEFERT, AND S. C. CARY. 2002. A continuous flow electrochemical cell for analysis of chemical species and ions at high pressure: Laboratory, shipboard and hydrothermal vent results, p. 54–72. *In* M. Taillefert and T. F. Rozan [eds.], *Environmental electrochemistry: Analyses of trace element biogeochemistry*. ACS Symposium Series. American Chemical Society.
- , P. J. BRENDEL, B. L. LEWIS, B. SUNDBY, L. LEFRANCOIS, N. SILVERBERG, AND D. B. NUZZO. 1998. Simultaneous measurement of O₂, Mn, Fe, I[–], and S(–II) in marine pore waters with a solid-state voltammetric microelectrode. *Limnol. Oceanogr.* **43**: 325–333.
- , AND T. M. CHURCH. 1988. Seasonal cycling of sulfur and iron in porewaters of a Delaware salt marsh. *Mar. Chem.* **23**: 295–309.
- , J. E. KOSTKA, T. M. CHURCH, B. SULZBERGER, AND W. STUMM. 1992. Seasonal iron cycling in the salt-marsh sedimentary environment: The importance of ligand complexes with Fe(II) and Fe(III) in the dissolution of Fe(III) minerals and pyrite, respectively. *Mar. Chem.* **40**: 81–103.
- , P. A. SHELLENBARGER, AND P. J. BRENDEL. 1996. Dissolved organic Fe(III) and Fe(II) complexes in salt marsh porewaters. *Geochim. Cosmochim. Acta* **60**: 951–960.
- MILLERO, F. J. 1986. The thermodynamics and kinetics of hydrogen sulfide system in natural waters. *Mar. Chem.* **18**: 121–127.
- MYERS, C. R., AND J. M. MYERS. 1993. Ferric reductase is associated with the membranes of anaerobically grown *Shewanella putrefaciens* MR-1. *FEMS Microbiol. Ecol.* **108**: 15–22.
- NEUHUBER, S. M. U. 2003. In situ measurements of redox chemical species with amperometric techniques to investigate the dynamics of biogeochemical processes in aquatic systems. M.S. thesis, School of Earth and Atmospheric Sciences, Georgia Institute of Technology.
- NEVIN, K. P., AND D. R. LOVLEY. 2002. Mechanisms for accessing insoluble Fe(III) oxide during dissimilatory Fe(III) reduction

- by *Geothrix fermentans*. *Appl. Environ. Microbiol.* **68**: 2294–2299.
- PEIFFER, S., M. DOS SANTOS AFONSO, B. WEHRLI, AND R. GACHTER. 1992. Kinetics and mechanism of the reaction of H₂S with Lepidocrocite. *Environ. Sci. Technol.* **26**: 2408–2413.
- POSTMA, D. 1985. Concentration of Mn and separation from Fe in sediments—I. Kinetics and stoichiometry of the reaction between birnessite and dissolved Fe(II) at 10°C. *Geochim. Cosmochim. Acta* **49**: 1023–1033.
- PYZIK, A. J., AND S. E. SOMMER. 1981. Sedimentary iron monosulfides: Kinetics and mechanism of formation. *Geochim. Cosmochim. Acta* **45**: 687–698.
- RICKARD, D. 1975. Kinetics and mechanism of pyrite formation at low temperatures. *Am. J. Sci.* **275**: 636–652.
- . 1995. Kinetics of FeS precipitation: Part 1. Competing reaction mechanisms. *Geochim. Cosmochim. Acta* **59**: 4367–4379.
- . 1997. Kinetics of formation of pyrite by the H₂S oxidation of iron(II) monosulfide in aqueous solutions between 25 and 125°C: The rate equation. *Geochim. Cosmochim. Acta* **61**: 115–134.
- , AND G. W. LUTHER III. 1997. Kinetics of pyrite formation by the H₂S oxidation of iron(II) monosulfide in aqueous solutions between 25 and 125°C: The mechanism. *Geochim. Cosmochim. Acta* **61**: 135–147.
- ROYCHOUDHURY, A. N., P. VAN CAPPELLEN, J. E. KOSTKA, AND E. VIOLLIER. 2003. Kinetics of microbially mediated reactions: Dissimilatory sulfate reduction in salt marsh sediments (Sapelo Island, Georgia, USA). *Estuar. Coast. Shelf Sci.* **56**: 1001–1010.
- , E. VIOLLIER, AND P. VAN CAPPELLEN. 1998. A plug flow-through reactor for studying biogeochemical reactions in undisturbed aquatic sediments. *Appl. Geochem.* **13**: 269–280.
- SASS, A. M., A. ESCHMANN, M. KUHL, R. THAR, H. SASS, AND H. CYPIONKA. 2002. Growth and chemosensory behavior of sulfate-reducing bacteria in oxygen-sulfide gradients. *FEMS Microbiol. Ecol.* **40**: 47–54.
- SCHOONEN, M. A. A., AND H. L. BARNES. 1991. Reactions forming pyrite and marcasite from solution. 2. Via FeS precursors below 100°C. *Geochim. Cosmochim. Acta* **55**: 1505–1514.
- SINGER, P. C., AND W. STUMM. 1970. Acidic mine drainage. Rate-determining step. *Science* **167**: 1121.
- STOOKEY, L. L. 1970. Ferrozine: A new spectrophotometric reagent for iron. *Anal. Chem.* **42**: 779–781.
- TAILLEFERT, M., A. B. BONO, AND G. W. LUTHER III. 2000. Reactivity of freshly formed Fe(III) in synthetic solutions and (pore)waters: Voltammetric evidence of an aging process. *Environ. Sci. Technol.* **34**: 2169–2177.
- , AND G. W. LUTHER III. 2000. The application of electrochemical tools for in-situ measurements in aquatic systems: A review. *Electroanal.* **12**: 401–412.
- , V. C. HOVER, T. F. ROZAN, S. M. THEBERGE, AND G. W. LUTHER III. 2002a. The influence of sulfides on soluble organic-Fe(III) in anoxic sediment porewaters. *Estuaries* **25**: 1088–1096.
- , AND T. F. ROZAN. 2002. Environmental electrochemistry: Analyses of trace element biogeochemistry. ACS Symposium Series, Vol. 811. Oxford University Press.
- , ———, B. T. GLAZER, J. HERSZAGE, R. E. TROUWBORST, AND G. W. LUTHER III. 2002b. Seasonal variations of soluble organic-Fe(III) in sediment porewaters as revealed by voltammetric microelectrodes, p. 247–264. *In* M. Taillefert and T. F. Rozan [eds.], *Environmental electrochemistry: Analyses of trace element biogeochemistry*. ACS Symposium Series, Vol. 811. Oxford University Press.
- THEBERGE, S. M., AND G. W. LUTHER III. 1997. Determination of the electrochemical properties of a soluble aqueous FeS species present in sulfidic solutions. *Aquat. Geochem.* **3**: 191–211.
- VAN CAPPELLEN, P., AND Y. WANG. 1996. Cycling of iron and manganese in surface sediments: A general theory for the coupled transport and reaction of carbon, oxygen, nitrogen, sulfur, iron, and manganese. *Am. J. Sci.* **296**: 197–243.
- VAN GENUCHTEN, M. T. 1981. Analytical solution for chemical transport with simultaneous adsorption, zero-order production and first order decay. *J. Hydrol.* **43**: 213–233.
- WANG, F., A. TESSIER, AND J. BUFFLE. 1998. Voltammetric determination of elemental sulfur in pore waters. *Limnol. Oceanogr.* **43**: 1353–1361.
- YAO, W., AND F. J. MILLERO. 1996. Oxidation of hydrogen sulfide by hydrous Fe(III) oxides in seawater. *Mar. Chem.* **52**: 1–16.

Received: 3 June 2004

Accepted: 15 February 2005

Amended: 8 March 2005